Astron. Astrophys. 324, 870–876 (1997)

ASTRONOMY
AND
ASTROPHYSICS

The X-ray jet and halo of NGC 6251

K.-H. Mack[1,⋆], **J. Kerp**[1,2], **and U. Klein**[1]

[1] Radioastronomisches Institut, Universität Bonn, Auf dem Hügel 71, D-53121 Bonn, Germany
[2] Max-Planck-Institut für Extraterrestrische Physik, Postfach 1603, D-85740 Garching, Germany

Received 14 June 1996 / Accepted 17 February 1997

Abstract. A new analysis of the *ROSAT* PSPC data of the giant radio galaxy NGC 6251 is presented. In supplement to the already published results we used a new approach to disclose the X-ray morphology of NGC 6251. We have detected an elliptically shaped X-ray halo out to a radial distance of about 100 kpc from the host galaxy. Moreover, we have discovered a close positional and intensity correlation of the radio continuum radiation of the jet with enhanced X-ray emission. Our analysis suggests that the bulk of the X-ray photons originates from a hot ($T \sim 10^7$ K) thin plasma, while Inverse-Compton scattering is not important. The X-ray plasma associated with the radio continuum jet is most likely confined by the magnetic lines of forces within the jet.

Key words: galaxies: individual: NGC 6251 – galaxies: jets – radio continuum: galaxies – X-rays: galaxies

1. Introduction

The giant radio jet of the E2-type galaxy NGC 6251 has been discovered in the radio continuum by Waggett et al. (1977). This jet is one of the brightest and most extended and was subject to various studies. At low and intermediate radio frequencies this source has been observed by Willis et al. (1978, 1982), Jägers (1987), and Willis & O'Dea (1990). In the frame of their radio continuum survey of giant radio galaxies Klein et al. (1994) extended the multi-frequency radio studies of NGC 6251 towards higher frequencies. High-resolution radio continuum observations disclosed a knotty structure of the inner jet region within 120″ of the radio core (Saunders et al. 1981; Perley et al. 1984, henceforth PBW84). Keel (1988) reported excess emission at optical wavelengths within the innermost, brightest part of the radio jet. It has a similar size as the radio knot and matches the estimates of flux densities and spectra derived in analogy to other optically observed jets.

Send offprint requests to: K.-H. Mack (Bologna address)
⋆ *Present address*: Istituto di Radioastronomia del CNR, Via P. Gobetti 101, I-40129 Bologna, Italy

Within the *Einstein* survey a host of extended X-ray halos around early-type galaxies has been detected with radial distances $\sim 40 - 70$ kpc from the cores of the galaxies (Fabbiano 1989, and references therein).

A detailed investigation of the X-ray properties of NGC 6251 was performed by Birkinshaw & Worrall (1993, henceforth BW93). They investigated the X-ray emission esp. of the host galaxy by analysing the entire *ROSAT* PSPC (Pfeffermann et al. 1986, Trümper 1983) energy window. The X-ray spectrum of the nucleus was found to be a composite of one or two different emitting processes. A flat-spectrum power-law component from the AGN plus the emission of a thermal plasma fit the *ROSAT* data best.

The existence of some extended X-ray emission surrounding the nucleus of NGC 6251 has already been mentioned by BW93. By fitting King-profiles to the *ROSAT* data they found indications of a galaxy halo extending out to some 75–100 kpc radius. Obviously, such an extended halo could strongly influence the morphology of the radio continuum radiation not only close to the nucleus but also of the extended structures like the outer jet or the radio lobes. In this respect, X-ray observations are an important tool to study the physical conditions around the galaxy nucleus and to explore the structure of the radio lobes far out in the intergalactic medium.

This paper presents a new analysis of the *ROSAT* PSPC data of NGC 6251 using an approach different from that of BW93. This also takes into account the progress of image processing of *ROSAT* observations during recent years. The analysis is described in Sect. 2, in Sect. 3 we present our results, which are summarized in Sect. 4. Throughout this paper we use $H_0 = 75\,\mathrm{km\,s^{-1}\,Mpc^{-1}}$ and $q_0 = 1$. The redshift of 0.0234 of NGC 6251 implies a distance of 91 Mpc.

2. Data analysis

We have extracted the pointed *ROSAT* PSPC observation of NGC 6251 from the public data archive of the Max-Planck-Institut für Extraterrestrische Physik in Garching. The observation was pointed at RA(2000) = $16^{\mathrm{h}}32^{\mathrm{m}}32\overset{\mathrm{s}}{.}0$ and DEC(2000) = $82^\circ32'16\overset{''}{.}4$. During the total integration time of 14.8 ksec the X-ray telescope performed a linear wobble motion around this

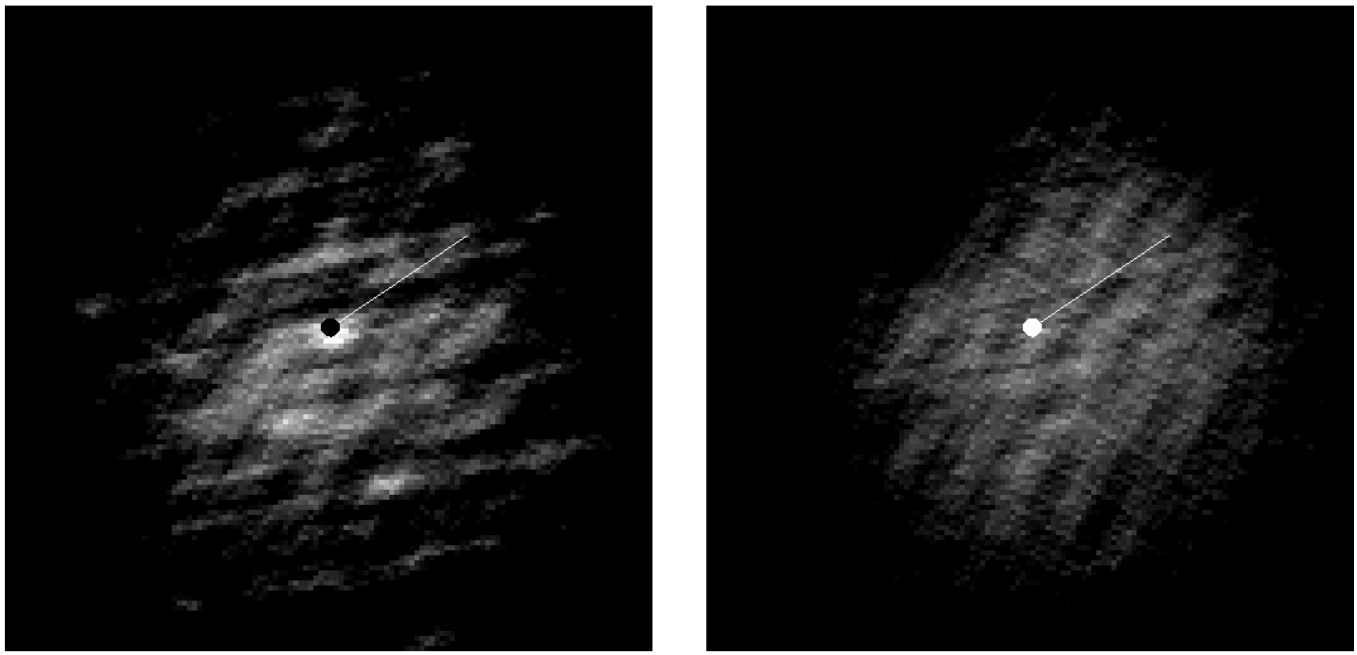

Fig. 1. a Merged exposure map of the entire *ROSAT* PSPC energy window (0.2 – 2.4 keV). The complex intensity structure of this map is caused by the convolution of the detector sensitivity map with the wobble motion of the X-ray telescope. The obvious irregularities in this map are dominantly caused by the ghost-image effect associated with very soft X-ray photons below $E \leq 0.28$ keV. The filled circle and the line indicate the position of NGC 6251 and the orientation of the radio jet. **b** Exposure map of the intermediate and hard energy band ranging from 0.5 – 2.4 keV.

central position to avoid constant shadowing by the detector support structure. Utilizing the program package EXSAS (Zimmermann et al. 1994) we split the photon events into three different energy bands. The soft band corresponds to the pulse-height-invariant (PI) energy channels 11–41 and is called the $\frac{1}{4}$ keV band. The PI channels 52–201 (H) cover the *ROSAT* $\frac{3}{4}$ keV (M-band, PI chan. 52–90) and 1.5 keV (J-band, PI chan. 91–201) energy bands (Snowden et al. 1994).

In the following we discuss the advantage of this separation of the photon events into different energy bands over the analysis of a single broad band covering the entire *ROSAT* energy window. As will be shown, this energy selection provides the opportunity to disclose the X-ray jet and halo of NGC 6251.

2.1. The X-ray data in different energy bands

Most of the photons detected within the *ROSAT* $\frac{1}{4}$ keV energy band are of Galactic origin. In the $\frac{1}{4}$ keV band the emission of the soft X-ray background (XRB) reaches its maximum. Consequently, the major fraction of photons is uncorrelated with the X-ray emission of NGC 6251.

Within the $\frac{3}{4}$ keV and 1.5 keV energy range the contribution of the XRB is nearly an order of magnitude lower (McCammon & Sanders 1990, Fabian & Barcons 1992). It is within these two harder bands that the structure of NGC 6251 becomes obvious.

The photoelectric absorption cross section of the Galactic interstellar matter rapidly decreases with increasing photon energy ($\sigma \sim \mathrm{E}^{-3}$; McCammon & Sanders 1990). Towards NGC 6251 the Galactic HI column density is $N_{\mathrm{HI}} = 5 \cdot 10^{20} \mathrm{cm}^{-2}$, taken from the survey of Hartmann & Burton (1997). This leads to an attenuation of 92% of the $\frac{1}{4}$ keV radiation by the Galactic interstellar matter, while in the $\frac{3}{4}$ keV band 33% and within the 1.5 keV band only 17% of the radiation is absorbed. Because of the strong X-ray background radiation and the attenuation we exclude the $\frac{1}{4}$ keV energy range from our analysis. In addition, not only the $\frac{1}{4}$ keV band alone is affected by these two serious problems but also any broad band *ROSAT* map as the following section will show.

2.2. The merged exposure maps

X-ray data from *ROSAT* have to be corrected for vignetting effects caused by mirror reflectivity and by obscuration of the detector support structure. This is performed by dividing the X-ray intensity maps by their corresponding merged exposure maps (Snowden et al. 1994). The merged exposure map is the convolution of the instrumental sensitivity map with the wobble motion of the X-ray telescope. Therefore, the intensity pattern of the merged exposure map is proportional to the sensitivity distribution of the entire PSPC pointed observation. Local maxima in the exposure map correspond to areas within the field of view where the PSPC detector is most sensitive during the observation. The $\frac{1}{4}$ keV range reveals the strongest deviation from an homogeneous sensitivity map. Since very low energy photons cannot induce signals in all cathode wires of the PSPC, the electronics can only define a probability cone for the direction from which

the photon encounters the detector. This so-called electronic ghost-image effect seriously reduces the angular resolution of the *ROSAT* X-ray telescope within the $\frac{1}{4}$ keV energy regime. Moreover, no analytic expression of the point-response function in the $\frac{1}{4}$ keV band can be given (Snowden et al. 1994). The ghost-image effect is also significant within the broad *ROSAT* energy band ranging from 0.2–2.4 keV. Fig. 1a displays the merged exposure map of the 0.2–2.4 keV energy range as a grey-scale image. The location of the core of NGC 6251 is marked by the black filled circle, while the orientation of the radio jet is indicated by the white line. Obviously, the merged exposure map of the full *ROSAT* energy band shows a complex intensity structure. Unfortunately, this broad-band exposure map reaches a local minimum towards the radio jet, while it is much brighter almost anywhere else. The evaluation of intensity differences within different map sectors centred on the galaxy nucleus (BW93) is dominated by the small scale structure of the exposure map. In particular, a broad sensitivity trough is crossing the jet (Fig. 1a) which leads to negative count rates and fluxes in these areas of the jet by evaluating ON and OFF intensity differences. This causes the non-detection of the X-ray emission associated with the radio jet of NGC 6251, which has been reported by BW93.

Fig. 1b shows the exposure map analysed in the present work. Again we indicate the core and the orientation of the radio jet of NGC 6251. This exposure map has a much smoother intensity structure than that covering the entire *ROSAT* energy range (Fig. 1a).

2.3. The non-cosmic backgrounds

Finally, we have investigated the influence of the so-called non-cosmic backgrounds on the X-ray data of NGC 6251. These non-cosmic backgrounds consist of scattered solar X-rays, long- and short-term enhancements (Snowden et al. 1994) and the particle background (Plucinsky et al. 1993). As mentioned in Sect. 2.2., they contribute most to the X-ray data just at the local intensity maxima of the merged exposure map. This can lead to artificially extended X-ray structures, which are statistically distributed across the field of view. In the worst case this can simulate an extended X-ray halo by the superposition of local maxima. With the exception of one component of the particle background, all of the non-cosmic background radiation encounters the PSPC detector via the entrance window. To overcome the non-cosmic backgrounds we cleaned the data for short-term enhancements and scattered solar X-ray using the method described by Kerp (1994). This leads to a reduction of the finally analysed integration time to 8.5 ksec. The significance of the data decreases accordingly by a factor of 1.3. We subtracted the particle background from the X-ray map 52–201, following the procedure described by Plucinsky et al. (1993). We are finally left with long-term enhancements which are dominant in the $\frac{1}{4}$ keV band. In the energy range analysed here they are an order of magnitude weaker (Snowden et al. 1994). Since the origin of these enhancements is unknown we can correct for its contribution only by subtracting a constant value across the entire field of view. The absolute value of the count rate is not important in our analysis because only intensity differences between the source and background are evaluated. Long-term enhancements are neglected at this point of the analysis.

The X-ray image of NGC 6251, corrected for the contribution of the non-cosmic backgrounds, reveals the same morphology of the X-ray halo and the jet as that only corrected by the merged exposure map (Fig. 2). This suggests that the small scale structure of NGC 6251 is not artificially caused by the non-cosmic backgrounds. Thus, accurate source fluxes can be obtained by merely evaluating the intensity difference between the ON and OFF source position after correcting for the merged exposure map.

In summary, we have analysed the hard part of the *ROSAT* PSPC data of NGC 6251 covered by the PI channels 52–201. This energy channel range roughly corresponds to the energy range of 0.5–2.0 keV and reveals the clearest picture of the extended X-ray structure of NGC 6251. In contrast to the analysis of the entire *ROSAT* PSPC energy window we exclude the contribution of the X-ray photons belonging in particular to the soft XRB, which accounts for $\sim 50\%$ of the detected photon events. The non-cosmic X-ray backgrounds are of negligible influence in the present analysis after correction of the X-ray map with the corresponding merged exposure map. The resulting maps, calibrated in [cts s^{-1} $arcmin^{-2}$] have been converted to yield flux densities in [Jy/b.a.]. To perform this conversion we transformed the X-ray intensity into units of [Jy/b.a.]:

$$[\mathrm{cts\,s^{-1}arcmin^{-2}}] = \mathrm{const} \cdot \overline{\mathrm{E}}^{-1} \cdot \mathrm{A_{eff}} \cdot (\mathrm{PSF})^{-2} \left[\frac{\mathrm{Jy}}{\mathrm{b.a.}}\right].$$

Here $\overline{\mathrm{E}}$ denotes the mean band energy of 1.23 keV and $\mathrm{A_{eff}}$ the mean effective area of 136 cm^2. The constant accounts for the transformation of [keV cm^{-2}] to [Jy] and is in our units equals $5.3 \cdot 10^5$. This conversion value also accounts for the photoelectric absorption of the X-ray photons by the galactic interstellar medium distributed along the line of sight. The X-ray flux is determined across an area enclosing the object of interest and covers, at least, the complete *ROSAT* point–response–function with PSF(FWHM) $\simeq 36''$ size averaged within the inner PSPC detector window. In general the X-ray flux integration area covers several *ROSAT* PSF areas to increase the statistical significance of the evaluted flux values.

3. Results and discussion

3.1. The X-ray halo

In Fig. 2 we show a grey-scale map of the X-ray emission at a mean *ROSAT* band energy of 1.23 keV. The superimposed contour lines represent the radio continuum emission at 10.6 GHz, obtained with the Effelsberg 100-m telescope (Klein et al. 1994). Within various OFF-positions (avoiding areas close to obviously significant X-ray emission) we have determined both the X-ray background and the noise level. The weakest displayed X-ray emission corresponds to 4σ. In Table 1 we have compiled regions with the closest neighbourhood of the core and jet of NGC 6251 which show significant X-ray emission on the one

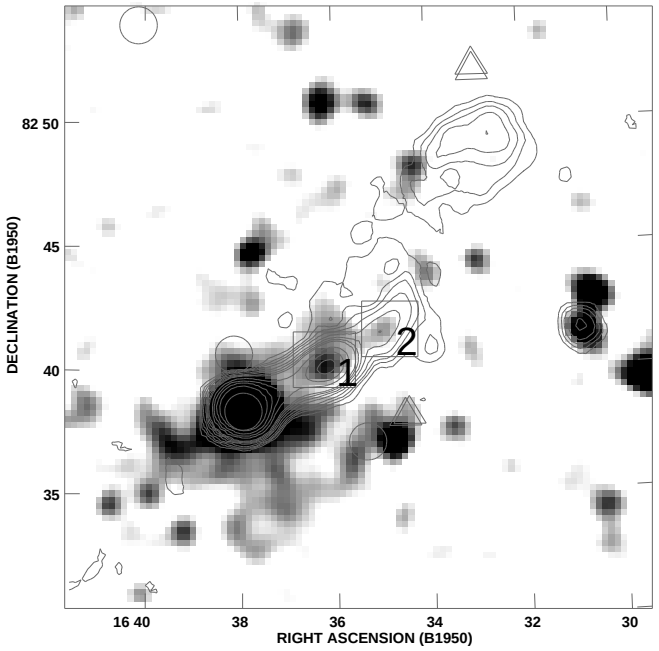

Fig. 2. Grey-scale map of the X-ray emission of NGC 6251. Darker grey means stronger emission. Superimposed as contours is the radio continuum emission at 10.6 GHz (Klein et al. 1994). Contour levels are 3, 5, 7, 10, 15, 20, 25, 30, 50, 70, 100, 150 mJy/beam. Both maps have the same resolution (69″). Boxes mark jet knots with positionally correlated X-ray and radio continuum excesses. Circles represent galaxies, triangles symbolize IRAS point sources found in the Simbad or NED database.

hand and are known to emit in the radio continuum on the other (Fig. 2 and the higher-resolution maps in Mack et al. 1997a). We have integrated the X-ray flux densities within rectangles around the centre coordinates given in Table 1.

The brightest X-ray feature is positionally coincident with the radio core of NGC 6251. The core of NGC 6251 is surrounded by extended (on arcmin scale) X-ray emission, which is probably the superposition of diffuse emission and point sources. In order to investigate the origin of the extended emission we have studied the Simbad and NED data bases to search for positional correlations between significant X-ray emission features and already identified objects (Fig. 2). The galaxy NGC 6252 north of NGC 6251, an IRAS source (IRAS 16344+8238) and another galaxy (NPM1G +82.0084) south-west of NGC 6251 could contribute to the detected X-ray emission (Table 1). However, no significant X-ray enhancements have been observed centred at the positions of these objects (Fig. 2). Rather, we find broad extended components which also cover these positions. Another X-ray/radio coincidence is obvious at RA: $16^{\rm h}31^{\rm m}$ and Dec: $82°41\farcm5$, west of the jet (Fig. 2). This source with an X-ray flux density of $(9.8 \pm 2.9) \cdot 10^{-9}$ Jy has been identified with 8C 1631+826 and is not related to NGC 6251 (Klein et al. 1994).

In order to improve our search for other positional coincidences of unknown X-ray emission with already identified objects we have performed a visual inspection of the Palomar Sky Survey which did not yield any identification. This suggests that most of the extended X-ray emission is in fact associated with NGC 6251. The bulk of the emission is most probably located close to, or even within, the large-scale halo of NGC 6251.

The global shape of the X-ray halo is elliptical (axis ratio: 1:0.6), with a position angle parallel to the direction of the radio jet. South of the core of NGC 6251 and its radio jet there is a striking protrusion in the X-ray emission, which gives the halo the asymmetric shape. The origin of the southern extension and the significant lack of X-ray emission west of the radio jet is still puzzling. The well-known radio lobes of NGC 6251 do not show significant extended X-ray emission. Comparing our X-ray data and the radio emission at low frequencies (e.g. PBW84) which trace the oldest, most extended regions of the radio lobes it is striking that the western radio lobe appears to expand just outside the X-ray halo.

3.2. The X-ray jet

The two brightest knots in the 10.6-GHz radio map (box 1 and 2 in Fig. 2) reveal a positional coincidence with excesses in the X-ray emission. Besides these, there also appears to be another coincidence at the counterjet side between radio and X-ray emission that cannot be found in the 10.6 GHz map, but becomes obvious at lower frequencies (e.g. at 1.4 GHz; PBW84).

In the following we focus to the two X-ray features which are positionally correlated with the bright knots of the radio jet. A priori, there are three main processes which can produce X-ray emission in radio galaxies: there are a few cases where synchrotron emission up to the X-ray regime has been found in jets (Vir A, Cen A, 3C273). Inverse-Compton scattering of cosmic microwave background photons to the X-ray regime by relativistic electrons is expected to take place in extended radio sources because of the large number of high energy electrons within the synchrotron-radiating regions and the ubiquity of low-energy photons provided by the cosmic microwave background. The first direct estimate of the magnetic field in a radio lobe, based on this process, has recently been reported by Feigelson et al. (1995). Finally, thermal X-ray emission produced by bremsstrahlung and line emission of hot thin plasmas are of importance to describe X-ray emitting objects. In the following we try to find out the relevant X-ray emission process.

3.2.1. Synchrotron emission?

We have integrated the X-ray and radio continuum intensities at the two brightest knots of the radio jet. Evaluating the radio continuum flux densities at 325 MHz, 608 MHz, and 10.6 GHz we have extrapolated the synchrotron emission to 1.5 keV, assuming a continuous injection model (Pacholczyk 1970) which is a reasonable scenario, for jet emission. The observed X-ray flux densities are higher than expected from the extrapolation. From these model fits we have determined break frequencies (Alexander & Leahy 1987) of 156 GHz and 257 GHz for the first and second knot, leading to mean particle ages of $6.6 \cdot 10^6$ yrs and

Table 1. X-ray enhancements in the NGC 6251 *ROSAT* PSPC observation

α_{50} h : m : s	δ_{50} ° : ′ : ″	possible identification	X-ray cts [cts s^{-1} arcmin^{-2}]	X-ray flux density [10^{-9} Jy]	EBR ($\frac{M}{H}$)
16 : 37 : 57	82 : 38 : 30	NGC 6251 core	$1.4 \cdot 10^{-2}$	311 ± 11	0.6 ± 0.1
16 : 36 : 06	82 : 40 : 40	NGC 6251 jet (1st knot)	$7.4 \cdot 10^{-4}$	13 ± 2	0.3 ± 0.2
16 : 35 : 04	82 : 41 : 40	NGC 6251 jet (2nd knot)	$5.2 \cdot 10^{-4}$	5 ± 1	0.6 ± 0.5
16 : 39 : 09	82 : 37 : 20	NGC 6251 counterjet	$8.3 \cdot 10^{-4}$	13 ± 2	0.9 ± 0.3
16 : 38 : 11	82 : 40 : 20	NGC 6252	$6.7 \cdot 10^{-4}$	7 ± 1	1.0 ± 0.8
16 : 34 : 50	82 : 37 : 20	IRAS source / galaxy	$1.2 \cdot 10^{-3}$	29 ± 3	0.7 ± 0.3

$8.9 \cdot 10^6$ yrs, respectively. The mean frequency of the analysed *ROSAT* band ($2.97 \cdot 10^{17}$ Hz) corresponds to electron energies of more than 10^{14} eV in an equipartition magnetic field of 5.9 μG and 1.9 μG in the two knots, respectively. The equipartition magnetic fields have been calculated as described in Sect. 3.2.2. The lifetime of such electrons is less than $3.5 \cdot 10^4$ yrs, which rules out the synchrotron process as the origin for the enhanced X-ray radiation of the jet, unless an effective re-acceleration scenario is invoked. Such a mechanism has been discussed for the jet of NGC 6251 by PBW84. Indeed, those authors found some indication for particle re-acceleration taking place in the region of the first knot between 174″ and 220″ from the core. However, the energy requirements for producing X-rays by synchrotron emission render this scenario unlikely. Therefore, the X-ray luminosity of the two prominent jet knots, though exceeding their extrapolated strengths, is most probably due to radiation processes other than synchrotron emission.

3.2.2. Inverse-Compton radiation?

We have calculated the magnetic field strength B_{IC} produced by the Inverse-Compton effect (see e.g. Harris & Grindlay 1979):

$$B_{IC}[G] = (1+z)^{\frac{\alpha+3}{\alpha+1}} (5.05 \cdot 10^4 \frac{\nu_R}{\nu_X})^{\frac{\alpha}{\alpha+1}} (5.75 \cdot 10^{-17} \frac{S_R}{S_X})^{\frac{1}{\alpha+1}}$$

where S_R and S_X are the flux densities (in Jy) at the frequency ν_R and ν_X (in GHz), respectively, z denotes the redshift of the source, and α is the spectral index ($S_\nu \sim \nu^{-\alpha}$).

For comparison the minimum energy magnetic field strength, B_{ME}, has been calculated using the formula of Miley (1980):

$$B_{ME}[G] = 6.94 \cdot 10^{-5} \left[(1+z)^{3+\alpha} \frac{S_R \nu_R^\alpha}{\Theta_X \Theta_Y s} \frac{\nu_2^{\frac{1}{2}-\alpha} - \nu_1^{\frac{1}{2}-\alpha}}{\frac{1}{2}-\alpha} \right]^{\frac{2}{7}}$$

Here Θ_X and Θ_Y are the angular extents of the source in X- and Y-direction (in arcsec), s is the path length through the source parallel to the line of sight (in kpc), and ν_1 and ν_2 are the upper and lower cutoff-frequencies (in GHz), typically taken equal to 0.01 GHz and 100 GHz, respectively. Both, the energy ratio of the heavy particles to that in the electrons and the filling factor have been assumed to be unity. We obtain $B_{IC} = 0.2\,\mu$G compared to a minimum energy magnetic field of $B_{ME} = 5.9\,\mu$G within the first knot ($\alpha = 0.59$) and $B_{IC} = 0.3\,\mu$G compared to $B_{ME} = 1.9\,\mu$G within the second one ($\alpha = 0.73$).

Although the free parameters in the equipartition formula yield a lower limit to the minimum energy magnetic field strength, the latter are significantly larger than the Inverse-Compton values. This suggests that the Inverse-Compton effect is not the dominant X-ray emission process in NGC 6251.

We have also derived a lower limit to the mean magnetic field strength within the radio lobes of NGC 6251 by inserting radio (325 MHz, Mack et al. 1997a) and X-ray flux densities, integrated across the area of the north-western lobe. We have excluded the jet, the hot spot region, and two background sources. With a flux density of 3.12 Jy at 325 MHz, an integrated X-ray flux density of $< 2.32 \cdot 10^{-7}$ Jy, and a spectral index of $\alpha = 1.2$ we obtain an average magnetic field within the north-western lobe of $B_{IC} \geq 0.35\,\mu$G. This value is strongly dependent on the spectral index. Then, $\alpha = 1.1\,(1.3)$ yields a magnetic field of $B_{IC} \geq 0.27\,(0.45)\mu$G. Compared with the lobe magnetic field of 0.3 μG derived from equipartition (Mack et al. 1997b) these values indicate that the radio lobes are not far from equipartition.

3.2.3. Thermal radiation?

Looking at the morphology (Fig. 2) of the synchrotron jet and the X-ray halo it is striking that the X-ray emission is extended, partly even exceeding the synchrotron contours. On the other hand it seems plausible that the halo gas is situated in a potential well encircling the galaxy. Obviously, it is not accidental that the shape of the halo is elliptical with its major axis along the orientation of the jet. Probably the jet forms a channel built up by magnetic fields along which the X-ray gas can propagate. Based on these considerations we will discuss the characteristics of a thermal gas coinciding with the two knots in the jet of NGC 6251. We have studied the spectrum of the extended X-ray emission by evaluating energy-band ratios (EBRs) between the *ROSAT* M and H band (Table 1). These ratios are only a rough approximation to real spectra, but they yield a useful

signal-to-noise ratio. Especially in case of the faint X-ray halo and the jet of NGC 6251 the analysis of energy band ratios is an advantageous method. In order to demonstrate the reliability of the procedure we also analysed the core of NGC 6251. The ratio, noted in Table 1, is in quantitative agreement with a power-law of $E^{-2\pm0.2}$, taking into account absorption by the Galactic neutral matter only. This finding corresponds to spectral fits performed by BW93.

Within the statistical uncertainties, the first and second knot of the X-ray jet show the same ratio. In addition, the counterjet reveals an energy band ratio which is also in agreement with the radiation of a hot thin plasma of $T_{plasma} \simeq 10^7$ K.

Assuming the X-ray radiation to be of thermal origin we can derive some properties of the plasma which we discuss in context with the radio data. The maximum halo density given by BW93 is $n \leq 10^{-4}\,cm^{-3}$, which leads to a pressure of $P_{plasma} \leq 1.4 \cdot 10^{-13}\,dyn\,cm^{-2}$. Taking into account that the existence of an X-ray emitting intergalactic medium is ruled out by the results of Hasinger et al. (1993) and the *COBE* measurements of the microwave background (Fabian & Barcons 1992), the pressure of the intergalactic medium with a density of $2 \cdot 10^{-6}\,cm^{-3}$ (Mack et al. 1997b) cannot confine the plasma within the jet. On the other hand, if we compare the thermal and magnetic energy density, $nkT = B^2/8\pi$, we obtain a magnetic field strength of $\leq 5\mu$G within the first knot and $\leq 3\mu$G within the second, applying densities as derived below. In the first knot the equipartition magnetic field slightly outweighs the derived magnetic field corresponding to thermal energy density. Hence, magnetic confinement could be responsible to collimate the jet of NGC 6251 up to the first knot. In the second knot it appears that the thermal energy density dominates the magnetic energy density. This could explain why the X-ray emitting gas is both weaker and restricted to a smaller channel within the jet. Beyond this second knot, assuming that the magnetic field strength decreases radially from the galaxy core, the synchrotron radiation of the jet drastically fades away and disappears in the diffuse extended emission of the huge north-western radio lobe. A weak remainder of the jet must continue, otherwise one would not expect to see the hot spot at the north-western edge of the lobe. Obviously the surrounding magnetic field strengths are not high enough to confine the X-ray gas any longer. The gas escapes the jet, which results in a decreasing emission measure.

At a temperature of $T_{plasma} \simeq 10^7$ K most of the energy losses of the hot plasma are caused by bremsstrahlung processes. Assuming a distance of 91 Mpc for NGC 6251 we can calculate the electron density n_e within the plasma (Fink & Trümper 1982),

$$n_e[cm^{-3}] = 2.04 \cdot 10^{13}\, L_B^{\frac{1}{2}}\, V^{-\frac{1}{2}}\, T^{-\frac{1}{4}},$$

where L_B denotes the total bremsstrahlung luminosity ($3.7 \cdot 10^{40} erg\,s^{-1}$ in the first, $1.2 \cdot 10^{39} erg\,s^{-1}$ in the second knot), V is the radiating volume ($9.5 \cdot 10^{69}$ cm^3 in the first, $2.4 \cdot 10^{69}$ cm^3 in the second knot). In both cases cylindrical geometry has been assumed. This yields $n_e \leq 7.2 \cdot 10^{-4}\,cm^{-3}$ and $n_e \leq 2.6 \cdot 10^{-4}\,cm^{-3}$ within the first and second knot, respectively. These numbers strongly depend on the size of the radiating volume. The cooling time, t_c, of such a plasma is (Fink & Trümper 1982)

$$t_c[s] = 2 \cdot 10^{11}\, T^{\frac{1}{2}}\, n_e^{-1}.$$

Using the numbers derived above we obtain $t_c > 10^{10}$ yrs. This suggests that the plasma can originate from the nucleus of NGC 6251 and can propagate along the direction of the radio jet. This could explain the elliptical shape of the halo with the major axis along the jet direction.

From depolarization and rotation measure analyses PBW84 concluded that there is no convincing evidence for any internal depolarization anywhere in the jet. Adopting the uniform slab model (Burn 1966) we have calculated the resulting depolarization, by inserting the parameters derived above into the equation:

$$DP = \frac{\sin(0.81 n_e B_{||} d\lambda^2)}{0.81 n_e B_{||} d\lambda^2}.$$

Here $B_{||}$ denotes the strength of the uniform magnetic field along the line of sight (in μG), d is the path length through the depolarizing medium (in pc), the wavelength λ is 18 cm, corresponding to the value used by PBW84 for their depolarization studies of the jet. Inspection of the radio continuum maps of PBW84 suggests a size of the knots of $\sim 10^4$ pc, half of which will contribute to the depolarization so that $d = 5 \cdot 10^3$ pc. The values derived above indicate that our results are consistent with the non-detection of the depolarization by PBW84. The thermal scenario for the X-ray emission of the jet and halo of NGC 6251 matches the observational constraints best. The jet plasma is most likely confined by the magnetic lines of forces out to the first knot. Beyond this point the magnetic field energy cannot exceed the plasma pressure, the magnetic field lines are widened up and the X-ray emission vanishes.

4. Summary

We have presented a new analysis of X-ray data of NGC 6251 taken from the *ROSAT* PSPC public archive. Extended X-ray emission around the nucleus of NGC 6251 has been found forming a sphere of at least 80 kpc radius. Moreover, X-ray emission positionally correlated with the radio jet, esp. with the two brightest parts of the outer jet, has been detected. This X-ray emission is still present out to a radial distance of 180 kpc from the galaxy centre.

We have investigated the origin of the X-ray emission. Synchrotron processes have been excluded because the lifetimes of the required electrons are so short that one would not expect to detect such electrons without effective re-acceleration mechanisms being at work. X-ray photons mainly resulting from Inverse-Compton scattering are ruled out as dominant process since the required magnetic field strengths are below the equipartition magnetic field. This means that thermal processes are most likely responsible for the detected X-ray emission. From energy-band ratios we derive a plasma temperature of $T \sim 10^7$ K. The pressure of the intergalactic medium is not sufficient to confine the detected X-ray emission of the jet of NGC 6251. Our analysis suggests that magnetic confinement is

a reasonable scenario, where the X-ray plasma is enclosed by the magnetic lines of forces parallel to the orientation of the radio jet. This is supported by several findings.

The low electron density of the gas provides cooling times which are long enough to detect X-ray emission so far away from the galaxy centre.

Along the bright parts of the radio jet (out to 140 kpc) the magnetic pressure in the jet is higher than that of the X-ray plasma. Further out, the predominant effect of the confining magnetic fields decreases until the magnetic fields cannot retain the X-ray gas. A comparison with depolarization studies shows the consistency of the derived densities and magnetic fields with the non-detection of the depolarization. All of these findings strongly suggest a thermal origin of the X-ray emission of the NGC 6251 halo and jet.

Acknowledgements. We are grateful to an anonymous referee who helped to improve the paper significantly. We thank W. Kundt and H. Lesch for helpful discussions. This research has made use of the NASA/IPAC Extragalactic Data Base (NED) which is operated by the Jet Propulsion Laboratory, California Institute of Technology, under contract with the National Aeronautics and Space Administration, and utilized the Simbad database, operated by CDS, Strasbourg, France. KHM and JK thank the Deutsche Forschungsgemeinschaft for financial support (grants KL533/4–2 and Me745/17–2).

References

Alexander P., Leahy J.P., 1987, MNRAS 225, 1
Birkinshaw M., Worrall D.M., 1993, ApJ 412, 568 (BW93)
Burn B.J., 1966, MNRAS 133, 67
Fabbiano G., 1989, ARAA 27, 87
Fabian A.C., Barcons X., 1992, ARAA 30, 429
Feigelson E.D., Laurent-Muehleisen S.A., Kollgaard R.I., Fomalont E.B., 1995, ApJ 449, L149
Fink H.H., Trümper J., 1982, in: Landolt-Börnstein VI, 2c, eds: Schaifers K., Voigt H.H., Springer, p. 33ff.
Harris D.E., Grindlay J.E., 1979, MNRAS 188, 25
Hartmann D., Burton W.B., 1997, Atlas of Galactic Neutral Hydrogen, Cambridge University Press
Hasinger G., Burg R., Giacconi R., Hartner G., Schmidt M., Trümper J., Zamorani G., 1993, A&A 275, 1
Jägers W.J., 1987, A&ASS 71, 75
Keel W.C., 1988, ApJ 329, 532
Kerp J., 1994, A&A 289, 597
Klein U., Mack K.-H., Strom R., Wielebinski R., Achatz U., 1994, A&A 283, 729
Mack K.-H., Klein U., O'Dea C.P., Willis A.G., 1997a, A&ASS, in press
Mack K.-H., Klein U., O'Dea C.P., Willis A.G., Saripalli L., 1997b, A&A, subm.
McCammon D., Sanders W.T., 1990, ARAA 28, 657
Miley G., 1980, ARAA 18, 165
Pacholzcyk A.G., 1970, Radio Astrophysics, Freeman & Co., San Francisco
Perley R.A., Bridle A.H., Willis A.G., 1984, ApJS 54, 291 (PBW84)
Pfeffermann E., Briel U.G., Hippmann H. et al. 1986, Proc. SPIE 733, 519
Plucinsky P.P., Snowden S.L., Briel U.G., Hasinger G., Pfeffermann E., 1993, ApJ 418, 519
Saunders R., Baldwin J.E., Pooley G.G., Warner P.J., 1981, MNRAS 197, 287
Snowden S.L., McCammon D., Burrows D.N., Mendenhall J.A., 1994, ApJ 424, 714
Trümper J., 1983, Adv. in Space Res. 2(4), 241
Waggett P.C., Warner P.J., Baldwin J.E., 1977, MNRAS 181, 465
Willis A.G., O'Dea C.P., 1990, Proc. IAU Symp. 140, 455
Willis A.G., Strom R.G., Perley R.A., Bridle A.H., 1982, Proc. IAU Symp. 141
Willis A.G., Wilson A.S., Strom R.G., 1978, A&A 66, L1
Zimmermann H.U., Becker W., Belloni T., Döbereiner S., Izzo C., Kahabka P., Schwentker O., 1994, MPE-Report 257

This article was processed by the author using Springer-Verlag LaTeX A&A style file *L-AA* version 3.